Canonical Wnt Signaling is Involved in Anterior Regeneration of the Annelid *Aeolosoma viride*

Cheng-Yi Chen[1, †], Wei-Ting Yueh[1, †], Jiun-Hong Chen[1, *]

[1] Department of Life Science, National Taiwan University, Taipei 10617, Taiwan (R.O.C.)

[†] These authors contributed equally to the manuscript

* Correspondence should be addressed to J-H. C. (chenjh@ntu.edu.tw)

Keywords: canonical Wnt signaling, annelid regeneration, blastema proliferation and differentiation

Funding: Undergraduate Student Joining Scientific Project of National Science Council, Taiwan (NSC 97—2815—C—002—033-B).

Abstract

Annelids are regenerative animals, but the underlying mechanisms await to be discovered. Because Wnt pathway is involved in animal regeneration to varying extents, we used *Aeolosoma viride* to interrogate whether and how this pathway plays a role in annelid anterior regeneration. We found that the expression of *wnt4*, *β-catenin* and nuclear-localized β-catenin protein were up-regulated during blastemal formation and down-regulated as anterior structures gradually reformed. Consistent with potential Wnt activities in the blastema, treatments with either Wnt pathway activator (azakenpaullone) or inhibitor (XAV939) inhibited head regeneration, which further supports a role of Wnt pathway during anterior regeneration. Detailed tissue-level examines demonstrated that wound closure and blastemal cell proliferation were impaired by over-activating the pathway, and that neuronal and musculature differentiation were affected under Wnt inhibition. Combined, gene expression and chemical inhibitor data suggest the presence of dynamic Wnt activities at different anterior regeneration stages: an initial low activity may be required for wound closure, and the following activation may signal blastemal formation and cell differentiation. In a nutshell, we propose that the canonical Wnt signaling regulates blastemal cellular responses during annelid regeneration.

Introduction

Among regeneration models, researches from hydra and planarian have uncovered many cellular and molecular mechanisms (King & Newmark, 2012; E. M. Tanaka & Reddien, 2011). To gain more perspectives into animal regeneration and to relate to broader evolutionary implications, researches in other emerging models are indispensable. Annelids are known for regeneration capabilities and some underlying mechanisms are evolutionarily shared with other animals. For example, similar to the neoblasts of planarian (King & Newmark, 2012; E. M. Tanaka & Reddien, 2011), *Enchytraeus japonensis* and *Pristina leidyi* maintain stem cells in every segment for regeneration (Myohara, 2012; Yoshida-Noro & Tochinai, 2010; Zattara, Turlington, & Bely, 2016). Proliferative stem cells of planarian and *Eisenia foetida* express pluripotent factors, such as *oct4*, *nanog* and *sox2* (Onal et al., 2012; Zheng, Shao, Diao, Li, & Han, 2016). Consistent with the requirement of innervation for vertebrate limb regeneration (Bryant, Endo, & Gardiner, 2002), diverted neuron fiber induces ectopic axis in *Eisenia* annelids (Bely, 2014). However, whether any molecular mechanism regulates annelid regeneration is not clear yet (Bely, 2014).

Canonical Wnt signaling pathway (i.e. the Wnt/β-catenin pathway) plays major roles in various regenerative models. In hydra, injury induced apoptosis triggers the secretion of wnt3 from dying cells and activates the oral pole regeneration (Chera et al., 2009). Knocking-down Wnt pathway genes affect the anterior-posterior axial registration during planarian regeneration (Augustin et al., 2006; Broun, Gee, Reinhardt, & Bode, 2005; Gurley, Rink, & Alvarado, 2008;

Iglesias, Gomez-Skarmeta, Saló, & Adell, 2008; King & Newmark, 2012; Lengfeld et al., 2009; Petersen & Reddien, 2008; E. Tanaka & Weidinger, 2008). Additionally, activating Wnt signaling enhances fin and limb regeneration in zebrafish and axolotl (Kawakami et al., 2006; Yokoyama, Ogino, Stoick-Cooper, Grainger, & Moon, 2007). In *Xenopus laevis,* activation of Wnt pathway rejuvenates the regenerative ability of aged limbs (Yokoyama et al., 2007). Therefore, Wnt pathway is likely to regulate regeneration in other models.

Here, we used an emerging annelid regeneration model *Aeolosoma viride* to interrogate the involvement of canonical Wnt pathway in annelid regeneration (C.-P. Chen et al., 2020). *A. viride* belongs to Aeolosomaitidae, Annelida, and is phylogenetically classified as "clitellate-like polychaetes" by morphological or molecular evidences (Hessling & Purschke, 2000; Zrzavý, Říha, Piálek, & Janouškovec, 2009). *A. viride* is a freshwater annelid, typically ranges 2-3 mm in length and 0.1-0.2 mm in width with brown spots scatter on its semitransparent epithelium. In lab conditions, *A. viride* only reproduce asexually by adding posterior segments, and the progeny detaches from the parent worm via paratomic fission (Falconi, Gugnali, & Zaccanti, 2015). Taking the advantage of its semitransparent appearance, we are able to directly observe its internal organs, such as horseshoe-shaped mouth and the digestive tract (Fig. 1A). In our preliminary tests, we found *A. viride* can robustly regenerate anterior segments in 5 days (C.-P. Chen et al., 2020). The posterior-most pygidium segment is hardly distinguishable from posterior wounds, resulting in biased assessment to successful regeneration. Therefore, we focused on anterior regeneration here.

In this report, we first showed transcriptional activation of *wnt4* and *β-catenin* during regeneration. Then, to assay Wnt pathway activity, we labeled nuclear localized β-catenin protein by immunohistochemistry. We found blastemal formation was accompanied with increasing levels of nuclear β-catenin between 12-24 HPA, which was followed by dropping levels of nuclear β-catenin when anterior structures gradually reformed. To functionally interrogate the pathway, we treated the worms with chemical inhibitors and found that both activating and inhibiting the pathway impaired regeneration. Further short-term treatments demonstrated that the chemical activator blocked wound closure and blastema formation; while the inhibitor affected neuron and muscle regeneration in the blastema. Lastly, we labeled proliferating cells and found that cell proliferation in wound tissue was inhibited when over-activating Wnt pathway. The dynamic changes of nuclear β-catenin level and discrete cellular responses under inhibitor treatments suggest that wound closure, blastemal formation and cell differentiation depends on mild activation of endogenous Wnt pathway. Tilting the balanced pathway activity to either extremity impaired complete tissue regeneration.

Results

Wnt pathway is activated in the regenerating blastema

To investigate whether Wnt pathway is involved in regeneration, we first tested the spatiotemporal expression patterns of *wnt4, wnt8* and *β-catenin* by whole-mount *in situ* hybridization (WMISH, Fig. 1). Upon amputation, the cutting plane was immediately covered by *wnt4* expressing epithelial cells (Fig. 1C). Then the epithelial *wnt4* signal diminished from the first hour-post-amputation (HPA) to 6 HPA before the gene was activated again at the wound from 12 HPA (Fig. 1D-F). The *wnt4* signal persisted in blastema until head structures completely reformed at 120 HPA (Fig. 1K). On the contrary, we did not detect significant up-regulation of *wnt8* throughout the repairing process (Fig. 1M-U'), suggesting preferential Wnt ligand activation during regeneration. *β-catenin* was activated from 24 HPA through 72 HPA and diminished when nascent head structures became recognizable at 96 HPA (Fig. 1DD).

Additionally, we observed *wnt4* and *β-catenin* expression at the posterior 1/4th segment of intact worms (Fig. 1B and V) where asexual fission occurs and EdU labeled proliferating cells are enriched (C.-P. Chen et al., 2020; Falconi et al., 2015) The expression of *wnt4* and *β-catenin* at this domain suggest that these genes may regulate the development of posterior growth zone, like other multipotent genes, such as *piwi*, *vasa* and *nanos* in other annelids (Gazave et al., 2013; Kozin & Kostyuchenko, 2015; Zheng et al., 2016).

In most studied models, active Wnt signaling cascade stabilizes cytoplasmic pool of β-catenin protein, which then translocate and accumulate in the nuclei and mediate downstream gene

119 transcription (Clevers & Nusse, 2012). We labeled β-catenin protein by immunohistochemistry
120 to evaluate the pathway activity during regeneration (Fig. 2). Combining with nuclear staining,
121 we found β-catenin localized in the nuclei of regenerating blastema (Fig. 2A-D). Because
122 nascent blastema was hardly distinguishable during early wound closure, we quantified the
123 ratio of β-catenin-enriched (β-catenin$^+$) nuclei to the blastemal nuclei from 12 HPA (Fig. 2R). We
124 found that when the proliferating blastema gradually became distinguishable from wound
125 epithelium between 12 to 24 HPA, the ratio of β-catenin$^+$ nuclei increased. Then the ratio of β-
126 catenin$^+$ nuclei decreased as head regeneration completed. Combined with ISH data, we
127 proposed that Wnt signaling is activated in the proliferating blastema from 12 HPA and is
128 gradually silenced until regeneration completes at 120 HPA.
129
130 **Perturbing Wnt pathway inhibited *A. viride* regeneration**
131 We next asked whether tuning Wnt pathway can modulate *A. viride* regeneration or not. To
132 further test the role of Wnt signaling in *A. viride* regeneration, we incubated amputated worms
133 in chemical activators: Wnt Agonist, Alsterpaullone (a GSK-3β inhibitor) and 1-azakenpaullone
134 (Azkp, a GSK-3β inhibitor) or inhibitor: XAV939 (XAV, a tankyrase inhibitor and, in turn stabilizes
135 axin Broun et al., 2005; Huang et al., 2009; Kunick, Lauenroth, Leost, Meijer, & Lemcke, 2004).
136 Since endogenous Wnt pathway was activated during blastemal initiation, we expected
137 chemically activating Wnt pathway may enhance blastemal proliferation. However, to our
138 surprise, these compounds inhibited *A. viride* regeneration in dose-dependent manners (Fig.
139 3A-D). For consistency, we applied 0.25 μM Azkp or 5 μM XAV in the following experiments. We
140 found smaller blastema of Azkp treated worms, suggesting over-activating Wnt pathway may

141 inhibit blastema formation (Fig. 3H-J). On the other hand, XAV did not affect blastema
142 formation (Fig. 3K-M), but worms did not regenerate prostomium (Fig. 3G, M).
143 Additionally, we validated the inhibitor effects by assaying the nuclear β-catenin level in Azkp or
144 XAV treated blastema (Fig. 2I-R). As expected, Azkp resulted in more nuclear localized β-catenin,
145 whereas XAV treated blastema showed less nuclear β-catenin than control at 24 and 48 HPA,
146 demonstrating the efficacy of these inhibitors.
147
148 In the above assays, we applied treatments throughout regeneration and found both Wnt
149 pathway activator and inhibitor impaired regeneration. From nuclear β-catenin level of control
150 worms, we found dynamic Wnt activities during regeneration. We hypothesized that different
151 Wnt pathway activities may be required at different regeneration stages. To test the hypothesis,
152 we applied 24H pulse of Azkp or XAV for detailed temporal examinations (Fig. 3N-O). We found
153 treatments of Azkp and XAV before 72 HPA resulted in greater incidences of defective
154 regeneration, suggesting the activity of Wnt pathway is required during early regeneration
155 stages. However, the two treatments showed different effective time windows: 0-24 HPA
156 amputees were sensitive to Azkp, while 24-48 HPA amputees were sensitive to XAV. Combining
157 nuclear β-catenin data with 24H pulse treatments, we propose that wound tissue may require
158 low Wnt pathway activities during initial 0-24 HPA and then high activities between 24-48 HPA.
159
160 **Perturbing Wnt pathway impaired neuron and muscle regeneration**
161 Our key criteria for assaying anterior regeneration of *A. viride* are the reformation of head
162 structures (the prostomium, the horseshoe-shaped mouth in the peristomium, Fig. 1) and free

gliding behavior on substrates. Since the majority of Azkp and XAV treated amputees failed to meet these criteria, we asked whether the neuron or muscle regeneration is impaired. We first examined the underlying innervation by immunolabeling acetylated α-tubulin (Fig. 4). After five days of regeneration, control *A. viride* recovered anterior neuron connections between the neuropils and the ventral nerve cords through the circumesophageal commissures, as well as dorsal-anterior sensory organs of the prostomium (Fig. 4A, D; Hessling & Purschke, 2000). Azkp treated worms failed to regenerate prostomium, and the ventral nerve cords of the remaining tissue showed degeneration and did not extend anteriorly to form circumesophageal commissures or neuropils (Fig. 4E, H). The XAV treated worms showed partial recovery of the neuron connection from the ventral nerve cords to the neuropil through the circumesophageal commissures (Fig. 4I, L). However, the prostomium and the innervation from neuropil to the dorsal-anterior sensory organs were missing, which may be the main reason for the failure of behavioral recovery.

The rhomboid shape-arrayed muscle net underlying the intact prostomium supports its flat shape and multi-directional movements (Fig. 4B). Such specialized musculature of prostomium can be distinguished from the rest of body segments, which is composed by the perpendicular-arrayed longitudinal and circular muscles. In addition to the observed neuronal regeneration defects, both Azkp- and XAV-treated worms did not regenerate the characteristic prostomium musculature (Fig. 4F, J), which further supported the observed regeneration defects from morphology and behavior.

Over-activating Wnt signaling by Azkp resulted in blastemal cell proliferation defects

From our previous report, we observed that wound blastema increased in size and showed the most cell proliferation between 24 and 48 HPA (Fig. 3E-G; C.-P. Chen et al., 2020). At the same stages, Azkp treated wound blastema did not show comparable size change like control or XAV treated worms (Fig. 3E-M). Despite Azkp and XAV treatments both inhibited anterior regeneration, subtle differential cellular responses to Wnt activity perturbation may exist. Because the blastema of Azkp treated wounds were smaller, we hypothesized that cell proliferation can be impaired in these worms. We first examined cumulative cell proliferation by 5-ethynyl-2'-deoxyuridine (EdU) pulse between 24 and 48 HPA (Fig. 5B, G, L). EdU^+ cells at the blastema were less condensed in Azkp treated worms than in control and XAV, suggesting that over-activating Wnt compromised blastemal cell proliferation and resulted in smaller blastema. Additionally, we observed that the EdU^+ cells were ectopically enriched in the 2^{nd} segment of Azkp treated worms (Fig. 5G). From single z section images, we found the secondary EdU^+ cell domain located at the anterior tip of the midgut (Fig. 5J), which was observed to lesser extents in control and XAV treated worms (Fig. 5E, O-P).

Additionally, we also labeled proliferating cells at 48 HPA by anti-phospho-histone 3 antibody (H3P, Fig. 5C, H, M). By quantifying the $H3P^+$ cells, we found the number of proliferating cells was significantly lower in the Azkp treated blastema than control and XAV treatments (Control: 55±33.4; Azkp: 18.8±8.2; XAV: 59.2±30.7; *p* of Control-Azkp = 0.01; *p* of Control-XAV = 0.89; *p* of Azkp-XAV = 0.001; Mann-Whitney U-test). Combining EdU and H3P assays, Azkp-induced

206 blastemal formation defects can be attributed to lacking proliferation at blastema and mis-

207 regulation of proliferating domain at the 2nd segment.

208

Discussion

In this report, we interrogated the involvement of Wnt pathway in *A. viride* anterior regeneration. Wnt pathway activities were dynamic during regeneration, with the highest activity at 24 HPA when the wound blastema was actively proliferating. Long term incubation with either chemical inhibitor or activator of Wnt pathway impaired regeneration. Further temporal experiments suggested the requirements for the relatively low Wnt activity between 0-24 HPA and high activity between 24-48 HPA. Examinations of innervation, musculature and cell proliferation revealed the underlying cellular responses under treatments. By integrating current observations, we provide the following reasonings about how Wnt pathway is involved in *A. viride* regeneration.

A. viride **regeneration depends on dynamic Wnt signaling activities**

The dynamic nuclear β-catenin levels suggest Wnt pathway activity varies through stages of *A. viride* regeneration. Thus, long-term treatments by either Azkp or XAV may counteract against endogenous Wnt activities at different stages and result in the ultimate regeneration failure. Then, we further narrowed the treatment into 24H pulses. We found that the two chemical inhibitors were effective before 72 HPA when normal wound tissue repaired through wound closure, blastemal formation and partial differentiation stages. Immediately after amputation, we observed that the wound was covered by nearby *wnt4* expressing epithelium, and then *wnt4* expression was down-regulated from 1 HPA until being activated again at the blastema from 12 HPA. Downregulation of *wnt4* at the wound site suggests that the wnt4-mediated Wnt signaling was silenced during wound healing. Therefore, Azkp treatment at this stage may

231 counteract the Wnt inactivation as well as compromise the following blastemal cell
232 proliferations. Alternatively, over-activating Wnt pathway may override endogenous activation
233 between 12-24 HPA and turn the tissue into non-permissive conditions for regeneration. Then,
234 XAV inhibited regeneration during 24-48 HPA when the most β-catenin accumulated in the
235 nuclei. Although blastemal proliferation was not affected by XAV, the underlying innervation
236 and prostomium musculature could not completely recover. Because the appearance of neuron
237 and muscle cells are signatures of blastemal cell differentiation from nascent stem cells, we
238 propose that the endogenous Wnt activation at 24 HPA can be required for blastemal cell
239 differentiation.
240
241 Collectively, as summarized in Fig. 6, our data suggest that the progression of regeneration is
242 dependent on different Wnt activities: wound closure and initial repairing occur under low Wnt
243 activity (0-24 HPA); high Wnt activity initiates blastemal proliferation (24 HPA); blastemal
244 differentiation requires median Wnt activity (24-48 HPA); continued completion of
245 regeneration after 72 HPA is inert to exogenous Wnt activity modulators.
246
247 **Wnt signaling may not regulate anterior-posterior identity of regenerating *A. viride***
248 Wnt pathway is indispensable for defining axis during embryogenesis and regeneration of many
249 animal models (Broun et al., 2005; Chera et al., 2009; Gurley et al., 2008; Iglesias et al., 2008;
250 Leclère, Bause, Sinigaglia, Steger, & Rentzsch, 2016; Lengfeld et al., 2009; Petersen & Reddien,
251 2008; E. Tanaka & Weidinger, 2008). In planarian, activating Wnt pathway promotes posterior
252 regeneration at the anterior wound; while inhibiting the pathway induces head formation at

the posterior wound (Iglesias et al., 2008; Petersen & Reddien, 2008). If axial patterning of Wnt pathway is evolutionarily conserved in *A. viride*, we anticipated that anterior regeneration would be enhanced when we inhibited the pathway, and that posterior regeneration would be enhanced when we over-activated the pathway. However, our current data and methods do not support such hypothesis, i.e. XAV did not enhance anterior regeneration. Additionally, we did not observe ectopic head regeneration from the posterior wounds from our preliminary XAV treatments. Prostomium and anterior neuronal regeneration were inhibited by XAV treatments, suggesting other side effects existed. On the other hand, anterior regeneration was inhibited when the pathway was over-activated by Azkp, but we could not confidently claim that these Azkp treated wounds were transformed to posterior identity for lacking axial markers. Therefore, labeling anterior-posterior molecular markers will be the future direction for testing whether Wnt pathway regulates the axial identity of regenerating *A. viride*.

GSK-3β activity is required for *A. viride* neuronal regeneration and maintenance

Innervation to the regenerating tissues can be necessary and sufficient for complete regeneration in many systems (A. Kumar & Brockes, 2012). For example, bisected salamander limbs cannot regenerate if the remaining neuron is removed (A. Kumar & Brockes, 2012); ectopic neuron growth initiates ectopic blastemal formation in annelids (Bely, 2014). In planarian, β-catenin-1 localizes in the nuclei of brain and ventral nerve cords and is required for brain patterning during regeneration (Hill & Petersen, 2015; Sureda-Gómez, Martín-Durán, & Adell, 2016). Azkp treatment results in neuronal regeneration defects in planarian, such as smaller cephalic ganglia and ectopically projected visual axons (Adell, Marsal, & Saló, 2008).

Consistent with this idea, the Azkp treated *A. viride* did not regenerate neurons and showed degenerating ventral nerve cords, suggesting the requirement of GSK-3β in neuronal regeneration and maintenance. On top of that, planarian neuron regeneration is required for blastemal morphogenesis (Adell et al., 2008). In *A. viride*, the blastemal cell proliferation and innervation were both impaired when GSK-3β was inhibited by Azkp, suggesting a linkage between neuron regeneration and blastema formation. If neuron is generally required for regeneration in diverse animal models, then it is likely that *A. viride* blastema formation can be also regulated by innervation, which possibly requires active GSK-3β. However, the epistatic or mutual regulation of innervation and blastema formation in *A. viride* is not clear yet and warrants further investigations.

In summary, we demonstrated that proper regulation of Wnt signaling activities is required for different stages of *A. viride* anterior regeneration. As an echo to other regeneration models, our data further generalize the involvement of Wnt signaling to regeneration in an evolutionarily conserved perspective. In the future, more sophisticate approaches, such as CRISPR/Cas9 mutagenesis, will provide detailed molecular mechanisms of annelid regeneration as well as comparative regeneration biology in a broader context.

Materials and methods

Animal husbandry

Animal husbandry followed Chen et al. 2020. The whole culturing colony was asexually descended from one single worm to avoid genetic differences.

Amputation

Before anterior amputation, *A. viride* was first bisected between the midgut and hindgut junction (Fig. 1A). By this method, we aimed to synchronize the posterior segments and to prevent any proliferating progeny interfering with assessing successful regeneration (C.-F. Chen, Sung, Chen, & Chen, 2018). During synchronization, *A. viride* was cultured in ASW at 25°C without feeding. The pygidium recovered in three days. Then, the anterior segments were amputated between the foregut and midgut junction (Fig. 1A).

By 144 hour-post-amputation (HPA), successful anterior regeneration was assessed by the following criteria: **1**) muscle contraction in prostomium and peristomium, **2**) appearance of horseshoe-shaped mouth (Fig. 1A); **3**) voluntary gliding behavior on substrates. Regeneration rates were assayed by averaging the proportion of successful regeneration worms form at least 3 biological replicates. Each replicate was started from >10 worms at 0 HPA.

Isolation of *A. viride wnt4*, *wnt8*, and *β-catenin* sequences

Total RNA of *A. viride* was purified from intact worms by TRIzol (Thermo Fisher Scientific; Waltham, MA) following manufacturer's instructions. Then, the cDNA library was reverse-

315 transcribed by SuperScriptIII Reverse Transcriptase (Thermo Fisher Scientific) with oligo dT as
316 the first strand primer. Using cDNA library as template and degenerated primers (Table 1), we
317 amplified target fragments by PCR, cloned the fragments into T&A™ vector (Yeastern Biotech
318 Co., Taiwan), and sequenced the insert fragment.
319
320 For 3' Rapid Amplification of cDNA Ends (3' RACE), the cDNA library was primed by 3' end
321 anchor primer (3' AP, Table 2). Then gene specific internal primers and 3' AP head primer were
322 used for nested PCR (Table S2). The amplified products were cloned into T&A™ vector and
323 sequenced.
324
325 To amplify the 5' end sequence, we performed 5' RACE by reverse transcribing the first strand
326 cDNA by gene specific primer (Table 2). Then multiple deoxycytidines were added to the 3' end
327 of cDNA by terminal deoxynucleotidyl transferase (ThermoFisher). The gene specific primers
328 and universal 5' end anchor primer (5' AP, Table 2) were used to amplify the 5' end sequence.
329 Secondary nested PCR with 5' AP head primer (Table 2) was used to further amplify the specific
330 sequence, which is followed by cloning and sequencing as described above.
331
332 **Gene homology analysis**
333 Thirteen subfamilies of Wnt homologues proteins were previously identified in
334 Lophotrochozoan genomes (Cho, Vallès, Giani, Seaver, & Weisblat, 2010; Prud'homme, Lartillot,
335 Balavoine, Adoutte, & Vervoort, 2002). To test the homology of *A. viride wnt* genes, we first
336 used SMART protein analysis (http://smart.embl.de/) to identify the WNT domain of

Lophotrochozaon Wnt genes and aligned them by the default parameter of MUSCLE of MEGA7 program (S. Kumar, Stecher, & Tamura, 2016). Then, the phylogenetic relationship of wnts were resolved by Neighbor-joining method by p-distance model with 10,000 bootstrap repeats clustering *A. viride wnt4* and *wnt8* within the corresponding subfamilies (Fig. 7).

The cloned β-catenin protein encodes 12 characteristic armadillo domains (ARM) by SMART analysis. The amino acid sequence of β-catenin showed higher similarity to *β-catenin* than *α-catenin* or *γ-catenin* homologs by NCBI protein BLAST, confirming the sequence identity as *Av-β-catenin*.

Chemical inhibitor treatments

Anterior amputated *A. viride* were washed with treatment solutions four times before incubating either through whole regeneration process (Fig. 3A-D) or at 24H intervals (Fig. 3N-O). 1-Azakenpaulone (Azkp; MilliporeSigma, Burlington, MA), XAV939 (XAV, MilliporeSigma), Alsterpaullone (MilliporeSigma), Wnt Agonist (MilliporeSigma) were dissolved in dimethyl sulfoxide (DMSO) as stock solutions, and then diluted in artificial spring water (ASW) as working solutions at designed concentrations. Control solution was prepared with comparable concentrations of DMSO in ASW.

Whole-mount Immunofluorescence (WMIF)

Worms were anesthetized by menthol saturated ASW, and then fixed with 4% PFA-ASW overnight at 4°C. Then the samples were washed 5 times with phosphate buffered saline (PBS,

pH=7.4) containing 0.1% Triton X-100 (PBST). After washing, the fixed worms were rinsed with 100% methanol 3 times at RT and stored at -20°C until proceeded to immunohistochemistry.

To begin immunohistochemistry, the samples were re-hydrated through series of 66% and 33% methanol in PBST washes and additional washes in PBST for 5 times. Then, the samples were treated with 5 µg/mL protease K solution at RT for 5 minutes, followed by incubation in 2 mg/mL glycine for 5 minutes and post-fixation with 4% PFA-PBST at RT for 1 hour. After post-fixation, the samples were washed 3 times with PBST, and immersed in the blocking solution (PBST with 3% bovine serum albumin and 5% Goat serum) for up to 1 hour at RT. Primary antibody incubation: Rabbit-anti-β-catenin antibody (in 1:800 dilution; MilliporeSigma, C2206), Rabbit-anti-H3P antibody (in 1:1000 dilution; MilliporeSigma, 06-570) or Mouse-anti-acetylated α-tubulin (in 1:1000 dilution; MilliporeSigma, T7451) was applied overnight at 4°C with blocking solution as diluent. After 6 times washing with PBST, samples were incubated in fluorophore conjugated Goat anti-Rabbit antibody or Goat anti-Mouse antibody (in 1:400 dilution; Thermo Fisher Scientific) for 2 hours at RT with blocking solution as diluent. F-Actin staining was performed on no methanol treated samples as follows: After 1 hour blocking by 1% BSA-PBST at RT, we incubated samples in BODIPY® FL Phallacidin (1:40 dilution in blocking buffer, Thermo Fisher Scientific) at RT for 1 hour. The nuclei were counter-stained with 1 µg/mL DAPI-PBST for 20 minutes at RT. After 4 times washes by PBST, the samples were immersed and cleared in 80% glycerol-PBS with 0.1% NaN_3 before mounting on slides.

Whole-mount *in situ* hybridization (WMISH)

381 DNA templates of riboprobes were amplified by gene specific primers (Table 3) and cloned into
382 T&A™ vector. After confirming the desired orientations by sequencing, we linearized the
383 plasmids as templates for DIG-labeled riboprobes synthesis by T7 polymerase (Thermo Fisher
384 Scientific) with DIG RNA labeling mix (MilliporeSigma).
385
386 The WMISH protocol was adopted from zebrafish WMISH protocol (Thisse & Thisse, 2008).
387 Sample preparation was similar to WMIF, but PBS with 0.1% Tween-20 (PBSTw) was used
388 instead of PBST. Pre-hybridization was performed in HYB^- buffer (50% formamide, 5X SSC, and
389 0.1% Tween-20 in DEPC-treated H_2O) at 65 °C for 1 hour. The riboprobes were diluted at 1
390 ng/µL in HYB^+ buffer (HYB^- buffer with 50 µg/mL Heparin and 0.5 mg/µL yeast tRNA;
391 MilliporeSigma). Hybridization was performed at 65 °C overnight. Then samples were washed at
392 65 °C by serial dilutions of HYB^- and 2X SSCTw (2X SSC with 0.1% Tween-20) from 2:1 to 1:2 ratio,
393 one 2X SSCTw wash, two 0.2X SSCTw (0.2X SSC with 0.1% Tween-20) washes, and another serial
394 dilution of 0.2X SSCTw and PBSTw from 2:1 to 1:2 ratio. The samples were washed once by
395 PBSTw at RT and immersed in blocking solution (5% BSA in PBSTw) at 4 °C overnight. The
396 samples were then incubated in 1:10,000 diluted anti-DIG-AP antibody (MilliporeSigma) in
397 blocking buffer at 4 °C overnight. Then samples were washed 10 times with PBSTw and 3 times
398 with AP buffer (0.1 M Tris-Cl, 0.05 M $MgCl_2$, 0.1 M NaCl and 0.1% Tween-20 in DEPC-treated
399 H_2O). NBT and BCIP were added in AP buffer for colorimetric reaction at 4 °C overnight. Finally,
400 the reaction was stopped by 5 times PBSTw washes and once 100% methanol wash before
401 immersing in 80% glycerol-PBS for mounting.
402

403 **EdU labeling**

404 Regenerating *A. viride* were incubated in 100 µM 5-ethynyl-2'-deoxyuridine (EdU; Thermo
405 Fisher Scientific) diluted in ASW from 24 to 48 HPA, when blastemal cells showed the most
406 proliferation (C.-P. Chen et al., 2020). Then, worms were anesthetized and fixed as WMIF
407 method. After protease K treatment and re-fixation, Click-iT® reaction was performed as
408 manufacturer's instruction (Click-iT® EdU Imaging Kits, Thermo Fisher Scientific). Experiments
409 validated the specificity of EdU is shown in Fig. 8.
410
411 **Microscopy**
412 Images of regenerating worms and *in situ* hybridization were taken by Stereo Investigator (MBF
413 Bioscience), Zeiss Axio Observer Z1 or Zeiss Axio Imager A1 microscope with a Zeiss AxioCam
414 MRc CCD camera. Fluorescent specimens were imaged by Leica TCS SP5 confocal laser scanning
415 microscope. Contrasts of images were adjusted as the corresponding control images by ImageJ.
416 Figures were prepared by Illustrator CC (Adobe).
417
418 **Image quantification**
419 β-catenin$^+$ and H3P$^+$ nuclei were manually quantified through z-stacks of regenerating blastema
420 by Fiji: in brief, the images were pre-processed by "Subtract Background", "Median" and the
421 nuclei were quantified by "3D Maxima Finder" (Boudier et al., 2013). EdU$^+$ nuclei quantification
422 was performed according to Cai et. al, 2009 with minor modifications (Cai, Vallis, & Reilly, 2009):
423 analysis of particles was set > 12 µm^2 corresponding to the cell size and covered the entire z
424 stack range of images.

425

426 **Statistic analysis**

427 Difference of successful regeneration rates were tested by Cochran Q test and McNemar
428 change test. The ratio of β-catenin^{+} nuclei was analyzed by two-tailed *t*-test, assuming equal
429 variances. Parametric unpaired *t*-test between treatments was performed for comparing the
430 ratio of EdU^{+} nuclei in blastema to 2nd segment with log-transformation. The number of H3P^{+}
431 nuclei in the blastema was assayed by Mann-Whitney U-test. *p* values less than 0.05 were
432 considered statistically significant.

433

434 # Declarations

435 **Ethics approval and consent to participate**

436 All experimental treatments on *A. viride* were approved by the Environmental Protection and
437 Occupational Safety and Health Center, National Taiwan University.

438

439 **Availability of data and material**

440 All data generated or analyzed during this study are included in this published article, or
441 available upon reasonable request from the corresponding author.

442

443 **Competing interests**

444 The authors declare that they have no competing interests

445

446 **Authors' contributions**

447 CYC, WTY and JHC prepared the manuscript. CYC and WTY design and perform the experiments
448 and analyzed the data. All authors read and approved the final manuscript.
449

450 **Acknowledgements**
451 We would like to thank Dr. Eric Hill from Stowers Institute for Medical Research, Kansas City,
452 MO for suggestions and critics on the manuscript. We appreciate Dr. Jr-Kai Yu from Institute of
453 Cellular and Organismic Biology, Academia Sinica, Taiwan, for kindly providing access to the
454 confocal microscopy.
455

References

Adell, T., Marsal, M., & Saló, E. (2008). Planarian GSK3s are involved in neural regeneration. *Development Genes and Evolution*, *218*(1–2), 89–103. https://doi.org/10.1007/s00427-007-0199-3

Augustin, R., Franke, A., Khalturin, K., Kiko, R., Siebert, S., Hemmrich, G., & Bosch, T. C. G. (2006). Dickkopf related genes are components of the positional value gradient in Hydra. *Developmental Biology*, *296*(1), 62–70. https://doi.org/10.1016/j.ydbio.2006.04.003

Bely, A. E. (2014). Early events in annelid regeneration: a cellular perspective. *Integrative and Comparative Biology*, *54*(4), 688–699. https://doi.org/10.1093/icb/icu109

Boudier, T., Ollion, J., Cochennec, J., Escude, C., Curie, M., Umr, C., … Paris, C. (2013). TANGO : a generic tool for high-throughput 3D image analysis for studying nuclear organization. *Bioinformatics*, *29*(14), 1840–1841. https://doi.org/10.1093/bioinformatics/btt276

Broun, M., Gee, L., Reinhardt, B., & Bode, H. R. (2005). Formation of the head organizer in hydra involves the canonical Wnt pathway. *Development*, *132*(12), 2907–2916. https://doi.org/10.1242/dev.01848

Bryant, S. V, Endo, T., & Gardiner, D. M. (2002). Vertebrate limb regeneration and the origin of limb stem cells. *The International Journal of Developmental Biology*, *46*(7), 887–896.

Cai, Z., Vallis, K. A., & Reilly, R. M. (2009). Computational analysis of the number, area and density of gamma-H2AX foci in breast cancer cells exposed to (111)In-DTPA-hEGF or gamma-rays using Image-J software. *International Journal of Radiation Biology*, *85*(3), 262–271. https://doi.org/10.1080/09553000902748757

478 Chen, C.-F., Sung, T.-L., Chen, L.-Y., & Chen, J.-H. (2018). Telomere maintenance during anterior
479 regeneration and aging in the freshwater annelid Aeolosoma viride. *Scientific Reports*, *8*(1),
480 18078. https://doi.org/10.1038/s41598-018-36396-y
481 Chen, C.-P., Fok, S. K.-W., Hsieh, Y.-W., Chen, C.-Y., Hsu, F.-M., Chang, Y.-H., & Chen, J.-H. (2020).
482 General characterization of regeneration in Aeolosoma viride (Annelida, Aeolosomatidae).
483 *Invertebrate Biology*, e12277. https://doi.org/10.1111/ivb.12277
484 Chera, S., Ghila, L., Dobretz, K., Wenger, Y., Bauer, C., Buzgariu, W., … Galliot, B. (2009).
485 Apoptotic cells provide an unexpected source of Wnt3 signaling to drive hydra head
486 regeneration. *Developmental Cell*, *17*(2), 279–289.
487 https://doi.org/10.1016/j.devcel.2009.07.014
488 Cho, S.-J. J., Vallès, Y., Giani, V. C., Seaver, E. C., & Weisblat, D. A. (2010). Evolutionary Dynamics
489 of the wnt Gene Family: A Lophotrochozoan Perspective. *Molecular Biology and Evolution*,
490 *27*(7), 1645–1658. https://doi.org/10.1093/molbev/msq052
491 Clevers, H., & Nusse, R. (2012). Wnt/β-catenin signaling and disease. *Cell*, *149*(6), 1192–1205.
492 https://doi.org/10.1016/j.cell.2012.05.012
493 Falconi, R., Gugnali, A., & Zaccanti, F. (2015). Quantitative observations on asexual reproduction
494 of Aeolosoma viride (Annelida, Aphanoneura). *Invertebrate Biology*, *134*(2), 151–161.
495 https://doi.org/10.1111/ivb.12087
496 Gazave, E., Béhague, J., Laplane, L., Guillou, A., Préau, L., Demilly, A., … Vervoort, M. (2013).
497 Posterior elongation in the annelid Platynereis dumerilii involves stem cells molecularly
498 related to primordial germ cells. *Developmental Biology*, *382*(1), 246–267.

499 Gurley, K., Rink, J., & Alvarado, A. (2008). Beta-catenin defines head versus tail identity during
500 planarian regeneration and homeostasis. *Science*, *319*(5861), 323–327.
501 https://doi.org/10.1126/science.1150029
502 Hessling, R., & Purschke, G. (2000). Immunohistochemical (cLSM) and ultrastructural analysis of
503 the central nervous system and sense organs in Aeolosoma hemprichi (Annelida,
504 Aeolosomatidae). *Zoomorphology*, *120*(2), 65–78. https://doi.org/10.1007/s004350000022
505 Hill, E. M., & Petersen, C. P. (2015). Wnt/Notum spatial feedback inhibition controls neoblast
506 differentiation to regulate reversible growth of the planarian brain. *Development*, *142*(24),
507 4217–4229. https://doi.org/10.1242/dev.123612
508 Huang, S.-M. A., Mishina, Y. M., Liu, S., Cheung, A., Stegmeier, F., Michaud, G. A., … Cong, F.
509 (2009). Tankyrase inhibition stabilizes axin and antagonizes Wnt signalling. *Nature*,
510 *461*(7264), 614. https://doi.org/10.1038/nature08356
511 Iglesias, M., Gomez-Skarmeta, J. L., Saló, E., & Adell, T. (2008). Silencing of Smed-betacatenin1
512 generates radial-like hypercephalized planarians. *Development*, *135*(7), 1215–1221.
513 https://doi.org/10.1242/dev.020289
514 Kawakami, Y., Esteban, C. R., Raya, M., Kawakami, H., Martí, M., Dubova, I., & Belmonte, J. C. I.
515 (2006). Wnt/beta-catenin signaling regulates vertebrate limb regeneration. *Genes Dev*,
516 *20*(23), 3232–3237. https://doi.org/10.1101/gad.1475106
517 King, R., & Newmark, P. (2012). The cell biology of regeneration. *Journal of Cell Biology*, *196*(5),
518 553–562. https://doi.org/10.1083/jcb.201105099

519 Kozin, V. V, & Kostyuchenko, R. P. (2015). Vasa, PL10, and Piwi gene expression during caudal
520 regeneration of the polychaete annelid Alitta virens. *Development Genes and Evolution*,
521 *225*(3), 129–138. https://doi.org/10.1007/s00427-015-0496-1
522 Kumar, A., & Brockes, J. P. (2012). Nerve dependence in tissue, organ, and appendage
523 regeneration. *Trends in Neurosciences*, *35*(11), 691–699.
524 https://doi.org/10.1016/j.tins.2012.08.003
525 Kumar, S., Stecher, G., & Tamura, K. (2016). MEGA7: Molecular Evolutionary Genetics Analysis
526 Version 7.0 for Bigger Datasets., *33*(7), 1870–1874.
527 https://doi.org/10.1093/molbev/msw054
528 Kunick, C., Lauenroth, K., Leost, M., Meijer, L., & Lemcke, T. (2004). 1-Azakenpaullone is a
529 selective inhibitor of glycogen synthase kinase-3. *Bioorganic & Medicinal Chemistry Letters*,
530 *14*(2), 413–416.
531 Leclère, L., Bause, M., Sinigaglia, C., Steger, J., & Rentzsch, F. (2016). Development of the aboral
532 domain in Nematostella requires β-catenin and the opposing activities of Six3/6 and
533 Frizzled5/8. *Development*, *143*(10), 1766–1777. https://doi.org/10.1242/dev.120931
534 Lengfeld, T., Watanabe, H., Simakov, O., Lindgens, D., Gee, L., Law, L., … Holstein, T. W. (2009).
535 Multiple Wnts are involved in Hydra organizer formation and regeneration. *Developmental*
536 *Biology*, *330*(1), 186–199. https://doi.org/10.1016/j.ydbio.2009.02.004
537 Myohara, M. (2012). What role do annelid neoblasts play? A comparison of the regeneration
538 patterns in a neoblast-bearing and a neoblast-lacking enchytraeid oligochaete. *PLoS One*,
539 *7*(5), e37319. https://doi.org/10.1371/journal.pone.0037319

Onal, P., Grün, D., Adamidi, C., Rybak, A., Solana, J., Mastrobuoni, G., … Rajewsky, N. (2012). Gene expression of pluripotency determinants is conserved between mammalian and planarian stem cells., *31*(12), 2755–2769. https://doi.org/10.1038/emboj.2012.110

Petersen, C. P., & Reddien, P. W. (2008). Smed-β-catenin-1 is required for anteroposterior blastema polarity in planarian regeneration. *Science*, *319*(5861), 327–330. https://doi.org/10.1126/science.1149943

Prud'homme, B., Lartillot, N., Balavoine, G., Adoutte, A., & Vervoort, M. (2002). Phylogenetic analysis of the Wnt gene family: insights from lophotrochozoan members, *12*(16), 1395–1400.

Sureda-Gómez, M., Martín-Durán, J. M., & Adell, T. (2016). Localization of planarian β-CATENIN-1 reveals multiple roles during anterior-posterior regeneration and organogenesis. *Development*, *143*(22), 4149–4160. https://doi.org/10.1242/dev.135152

Tanaka, E. M., & Reddien, P. W. (2011). The cellular basis for animal regeneration. *Devlopmental Cell*, *21*(1), 172–185. https://doi.org/10.1016/j.devcel.2011.06.016

Tanaka, E., & Weidinger, G. (2008). Heads or tails: can Wnt tell which one is up? *Nature Cell Biology*, *10*(2), 122–124. https://doi.org/10.1038/ncb0208-122

Thisse, C., & Thisse, B. (2008). High-resolution in situ hybridization to whole-mount zebrafish embryos. *Nature Protocols*, *3*(1), 59–69. https://doi.org/10.1038/nprot.2007.514

Yokoyama, H., Ogino, H., Stoick-Cooper, C. L., Grainger, R. M., & Moon, R. T. (2007). Wnt/beta-catenin signaling has an essential role in the initiation of limb regeneration. *Developmental Biology*, *306*(1), 170–178.

561 Yoshida-Noro, C., & Tochinai, S. (2010). Stem cell system in asexual and sexual reproduction of
562 Enchytraeus japonensis (Oligochaeta, Annelida). *Development, Groth & Differentiation*,
563 *52*(1), 43–55. https://doi.org/10.1111/j.1440-169X.2009.01149.x
564 Zattara, E. E., Turlington, K. W., & Bely, A. E. (2016). Long-term time-lapse live imaging reveals
565 extensive cell migration during annelid regeneration. *BMC Developmental Biology*, *16*(6).
566 https://doi.org/10.1186/s12861-016-0104-2.
567 Zheng, P., Shao, Q., Diao, X., Li, Z., & Han, Q. (2016). Expression of stem cell pluripotency factors
568 during regeneration in the earthworm Eisenia foetida. *Gene*, *575*(1), 58–65.
569 https://doi.org/10.1016/j.gene.2015.08.034.
570 Zrzavý, J., Říha, P., Piálek, L., & Janouškovec, J. (2009). Phylogeny of Annelida (Lophotrochozoa):
571 Total-evidence analysis of morphology and six genes. *BMC Evolutionary Biology*, *9*(1), 1–14.
572 https://doi.org/10.1186/1471-2148-9-189
573

574

575 # Figures

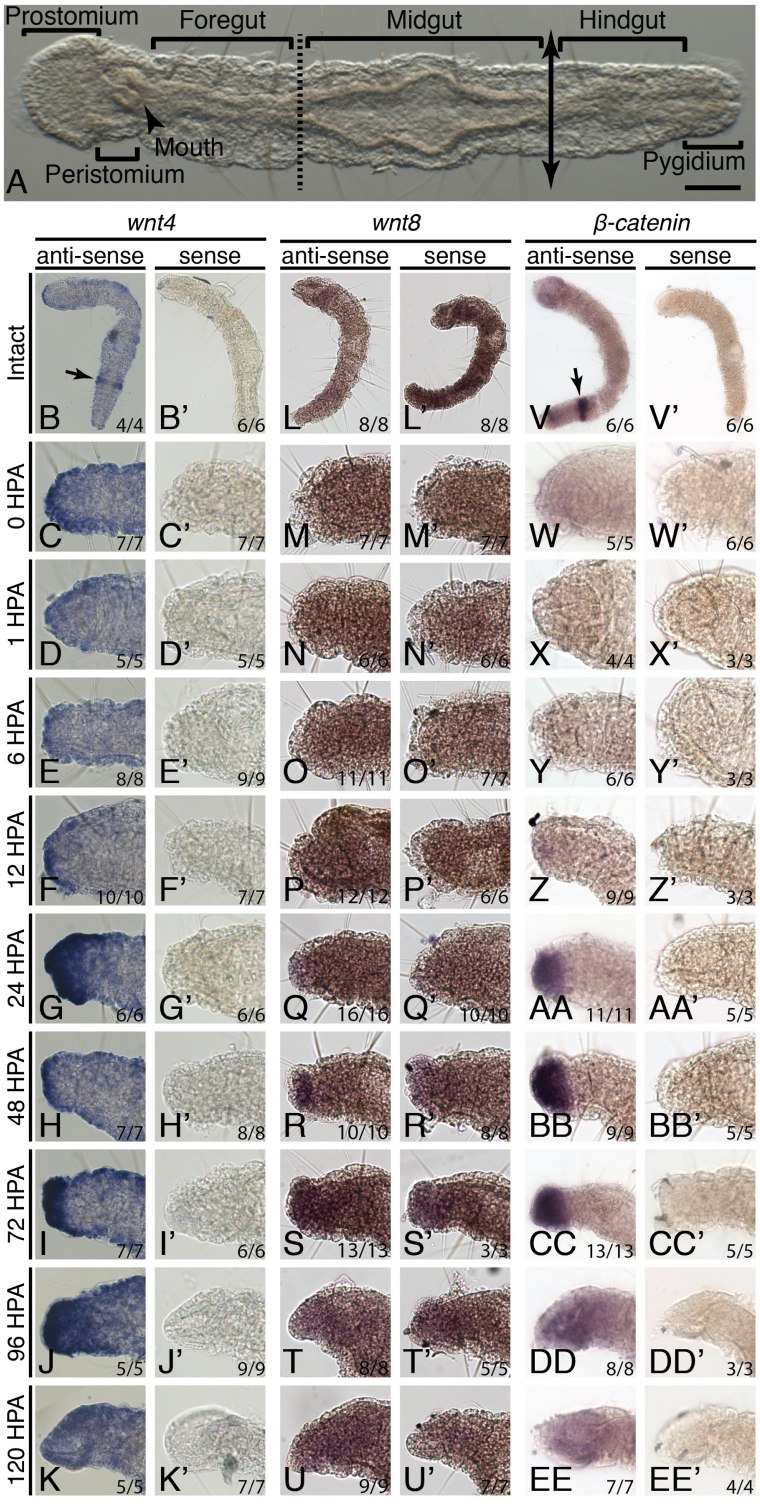

576

Fig. 1. Regenerating wounds show *wnt4* and *β-catenin* activation during blastemal cell proliferation. (**A**) Dorsal view of an intact worm. Double arrow line indicates posterior synchronizing cutting plane between midgut and hindgut junction. Dotted line indicates the anterior amputation plane between foregut and midgut junction. (**C**-**K'**) *wnt4* expression pattern during regeneration. Epithelial *wnt4* signal decreased within the first 6 HPA (**C**-**E**), followed by activation in the blastema between 24-96 HPA (**G**-**J**). (**M**-**U'**) *wnt8* expression in the blastema was indistinguishable from background signals. (**W**-**EE'**) *β-catenin* expression pattern during regeneration. *β-catenin* was activated in the blastema between 24-72 HPA (**AA**-**CC**). In intact worms, *wnt4* and *β-catenin* could be detected at the posterior proliferating segments of intact worms (arrows of **B** and **V**). Ratio at the lower right corner indicates specimens showing the corresponding expression patterns. Scale bar in **A** = 100 µm.

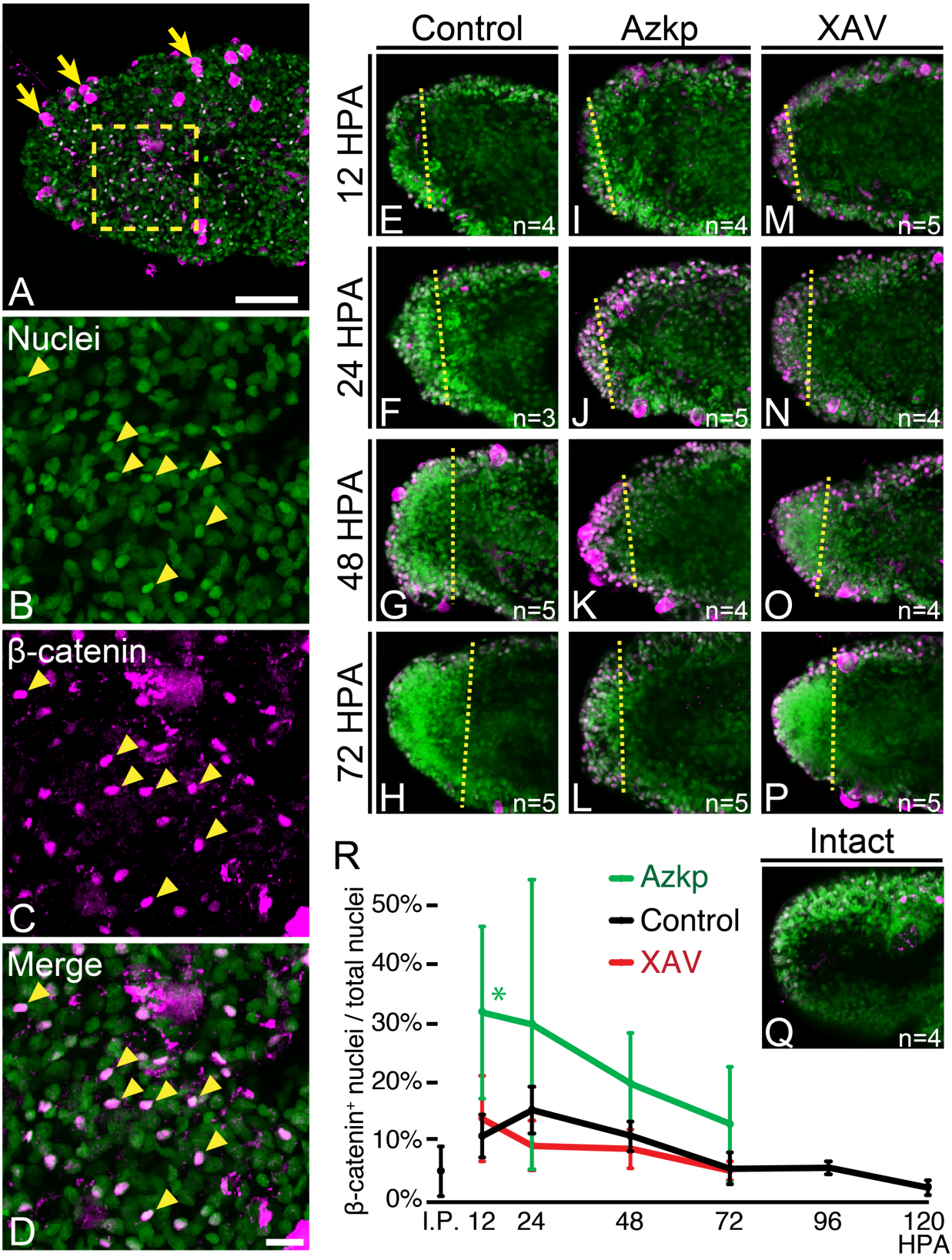

589

590 **Fig. 2. Nuclear β-catenin suggests Wnt pathway activation during blastemal proliferation at**
591 **24 HPA.** (**A**-**D**) Ventral view of 24 HPA blastema shows β-catenin protein (*magenta*)
592 accumulated in some nuclei (*green*) as indicated by arrowheads. Some non-specific signals were
593 also detected on the epithelium (arrows). (**B**-**D**) Higher magnification of the box region in **A**. (**E**-
594 **P**) Representative images of nuclear β-catenin at regeneration stages under control or inhibitor
595 treatments. (**Q**) Intact prostomium of β-catenin immunohistochemistry stain. (**R**) The ratio of β-
596 catenin^{+} nuclei to total blastemal nuclei under different conditions. Control blastema showed
597 highest level of β-catenin^{+} at 24 HPA. Azkp enhanced nuclear β-catenin level (*green* line), while
598 XAV down-regulated nuclear β-catenin level at 24 and 48 HPA (*red* line). **E**-**Q** are maximum
599 projections from ten serial focal planes. Error bars represent the standard deviation of the
600 mean from >3 worms. I.P. = Intact prostomium. Scale bar of **C** = 100 µm; **C'** = 10 µm. *Yellow*
601 dotted lines of **E**-**P** indicate the amputation plane. * denotes $p<0.05$ of *t*-test compared with
602 control at the corresponding time point.
603

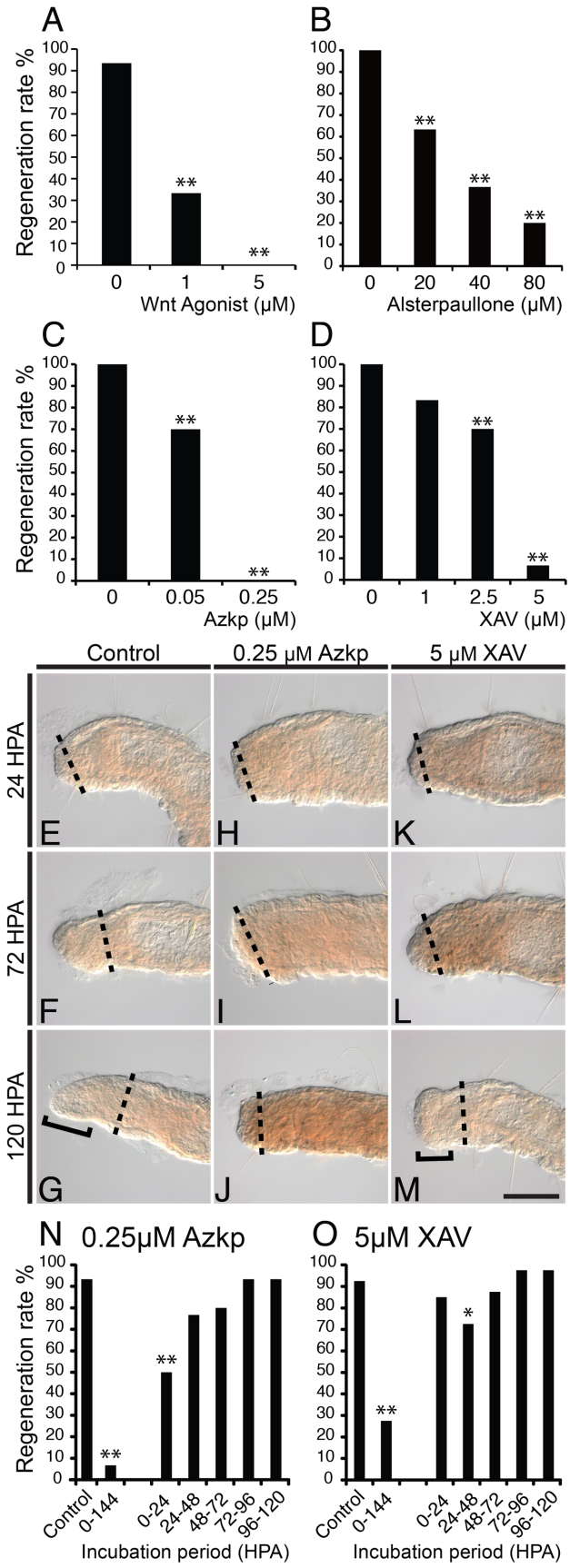

604

Fig. 3. Over-activating and down-regulating Wnt pathway both inhibited regeneration. (**A**-**D**) Exogenous Wnt pathway activators (Wnt agonist, Alsterpaullone and Azakenpaullone), and inhibitor (XAV939), inhibited regeneration in dose-dependent manners. (**E**-**M**) Lateral view of regeneration stages under control, 0.25 µM Azkp or 5 µM XAV treatments. Azkp treated worms showed smaller blastema (**H**-**J**). XAV939 did not affect blastema formation (**K**-**M**), but worms did not regenerate prostomium (compare bracket regions of **G** and **M**). (**N**-**O**) Successful regeneration rates under 24H pulses. Regeneration was significantly inhibited by 0.25 µM Azkp treatment between 0-24 HPA (**N**), and by 5 µM XAV treatment between 24-48 HPA XAV (**O**). Anterior end is toward the left and dorsal to the top. Dotted lines indicate cutting planes. Scale bar in **M** = 100 µm. All images are at the same scale. * denotes $p<0.05$. ** denotes $p<0.01$.

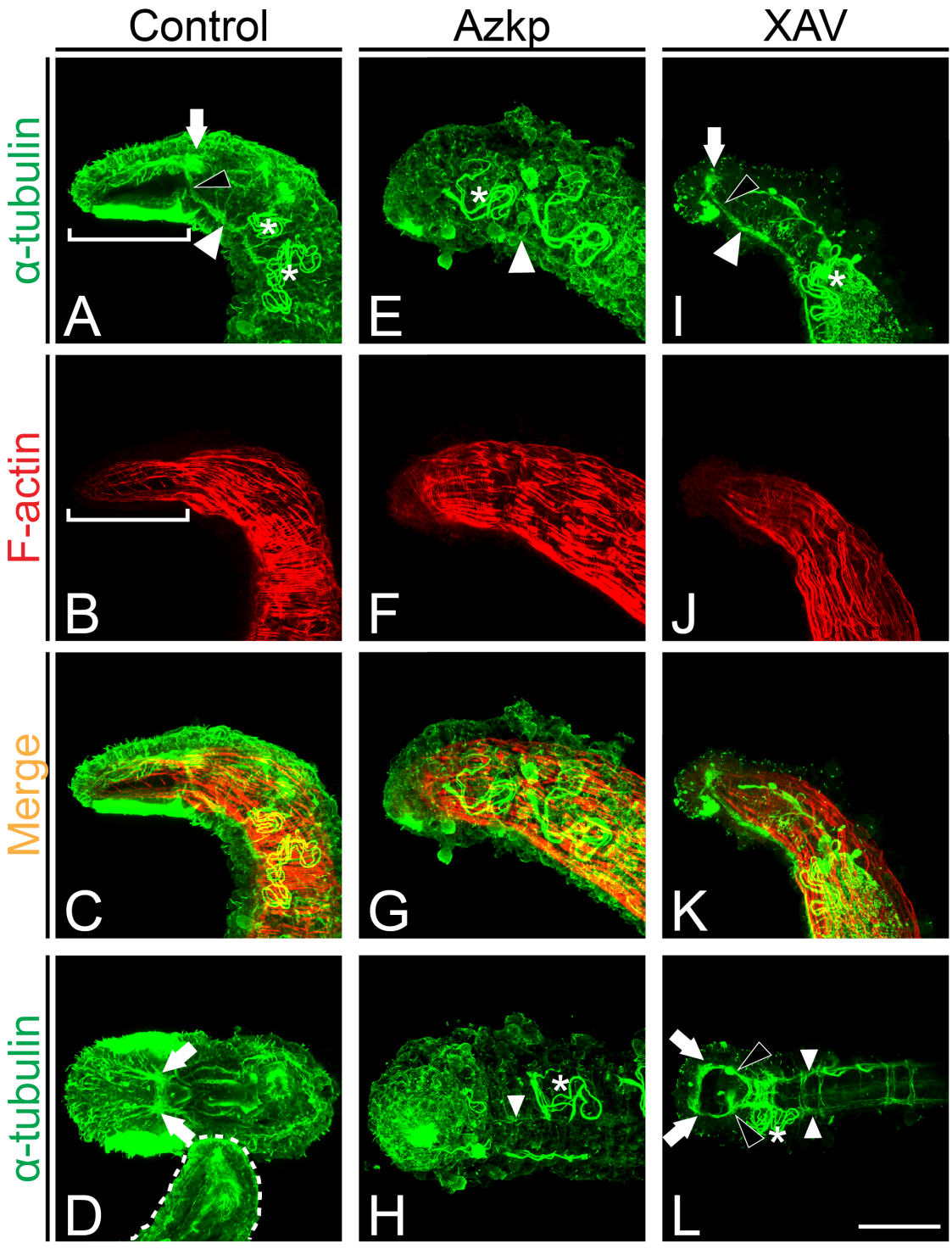

Fig. 4. Over-activating Wnt pathway inhibited neuron regeneration and maintenance. (**A**-**D**) By 144 HPA, control worms showed recovered innervation (acetylated α-tubulin, *green*) with neuropil in the prostomium (*white* arrows) connecting to the ventral nerve cord (*white*

arrowhead) by the circumesophageal commissures (*black* arrowhead). The neuropil extended exons dorsal-anteriorly to the epithelial sensory cilia. Ventral prostomial ciliary field was also enriched with acetylated α-tubulin (bracket of **A**). Rhomboid shape-arrayed muscle net (F-actin, *red*) supported the flat prostomium (bracket region of **B**). The *white* dotted line in **D** delineates the pygidium of the worm. (**E**-**H**) Azkp treated worms did not regenerate anterior innervations from the degenerated ventral nerve cord (*white* arrowheads) and the prostomium (**F**). (**I**-**L**) XAV treated worms regenerated anterior innervation where the neuropil (*white* arrows) and circumesophageal commissures (*black* arrowheads) connect to the ventral nerve cords (*white* arrowheads). However, these worms did not regenerate the prostomium (**J**). Asterisks indicate metanephridia. Anterior of all amputees are toward the left. Figure **A**-**C**, **E**-**G**, and **I**-**K** are lateral views with dorsal to the top. Figure **D** is dorsal view; **H** and **L** are ventral views. Scale bar in **L** =100 µm. All images are at the same scale.

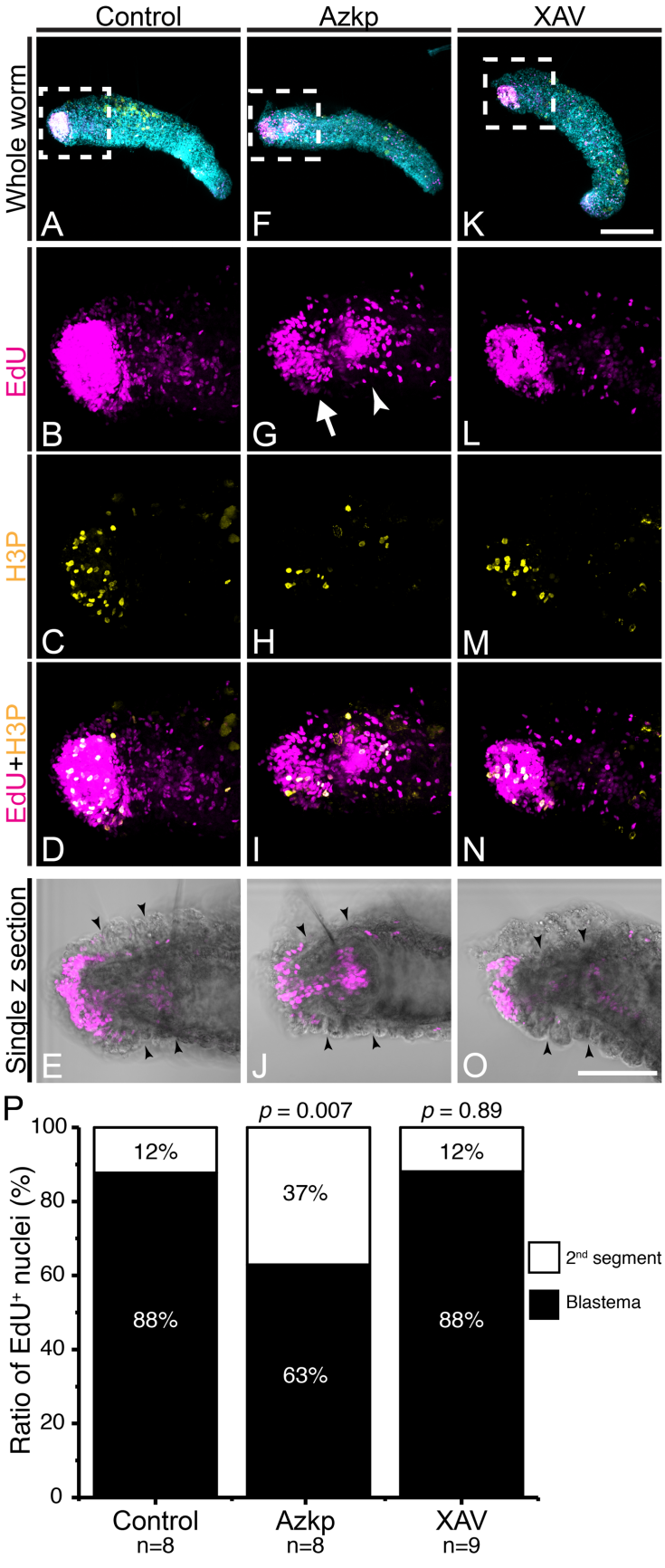

633

634 **Fig. 5. Over-activating Wnt pathway impaired blastemal cell proliferation.** (**A**-**O**) Proliferating
635 cells between 24 to 48 HPA are labeled by EdU (*magenta*) or anti-H3P antibody (*yellow*). The
636 nuclei are false-colored in *cyan*. Higher magnification views of *white* rectangle areas of **A**, **F** and
637 **K** are in the corresponding lower panels. In control and XAV treated worms, active proliferating
638 blastema showed condensed EdU signals (**B** and **L**); while Azkp treatment resulted in less EdU^+
639 nuclei at the wound site (arrow) and a second domain of proliferating cells in the 2^{nd} segment
640 (arrowhead, **G**). (**J**) Single z section image shows that the proliferating cells in the 2^{nd} segment
641 were located at the front end of midgut. Anterior of all amputees are toward the left with
642 dorsal to the top. Black arrowheads in **E**, **J** and **O** delineate the blastema and the segment
643 boundary. (**P**) Ratio of EdU^+ nuclei between blastema and the following 2^{nd} segment. Student *t*-
644 test comparison with control worms shows significant ($p = 0.007$) enrichment of EdU^+ nuclei at
645 the 2^{nd} segment of Azkp treated blastema. Scale bar in **K** = 200 µm; **O** = 100 µm. **A**, **F** and **K** are
646 at the same scale. **B-E**, **G-J** and **L-O** are at the same scale.
647

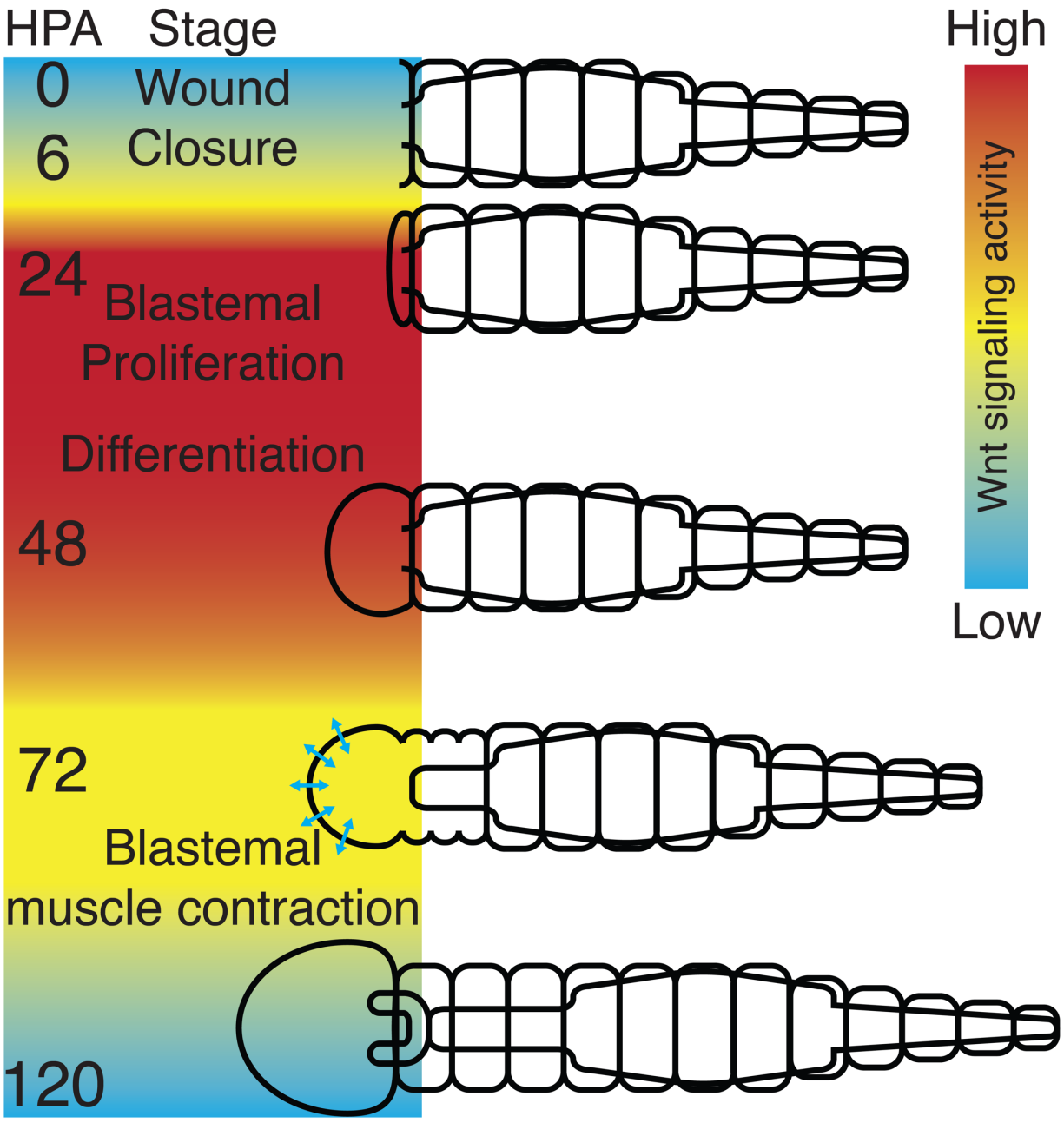

Fig. 6. A proposed model of endogenous Wnt pathway activity during *A. viride* regeneration. A rainbow pallet defines hypothesized blastemal Wnt activities. After amputation, wound closure finishes in the first 6 HPA. Then blastema gradually enlarges at the wound site by cell proliferation. By 72 HPA, blastemal tissue initiates occasional contraction, indicating neuron

654 and muscle cell differentiation. By 120 HPA, worms complete regeneration with a horseshoe-

655 shaped mouth and can freely glide on substrates.

656

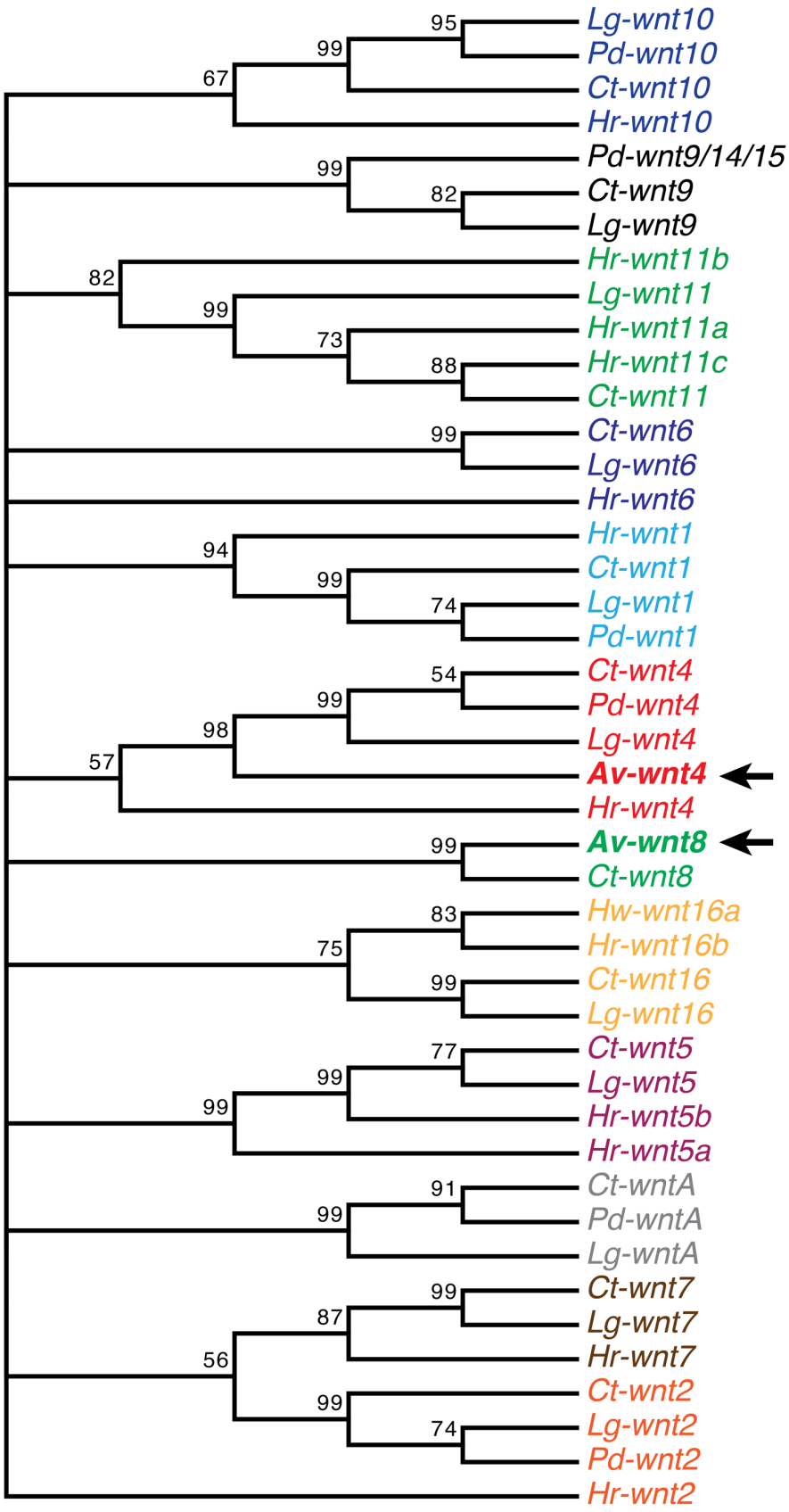

657

658 **Fig. 7. Neighbor-joining tree clusters *A. viride wnt* genes into the corresponding**

659 **Lophotrochozoan *wnt* subfamilies.** *Av-wnt4* and *Av-wnt8* are indicated by arrows. Within the

660 10,000 replicates bootstrap tests, the percentage of replicate trees in which the associated taxa

661 clustered together are shown at the branches. Note that the nodes with bootstrap percentage

662 <50% are compressed. Species name abbreviations: *Av: Aeolosoma viride*; *Ct*: *Capitella teleta*;

663 *Hr*: *Helobdella robusta*; *Lg*: *Lottia gigantea*; *Pd*: *Platynereis dumerilii*.

664

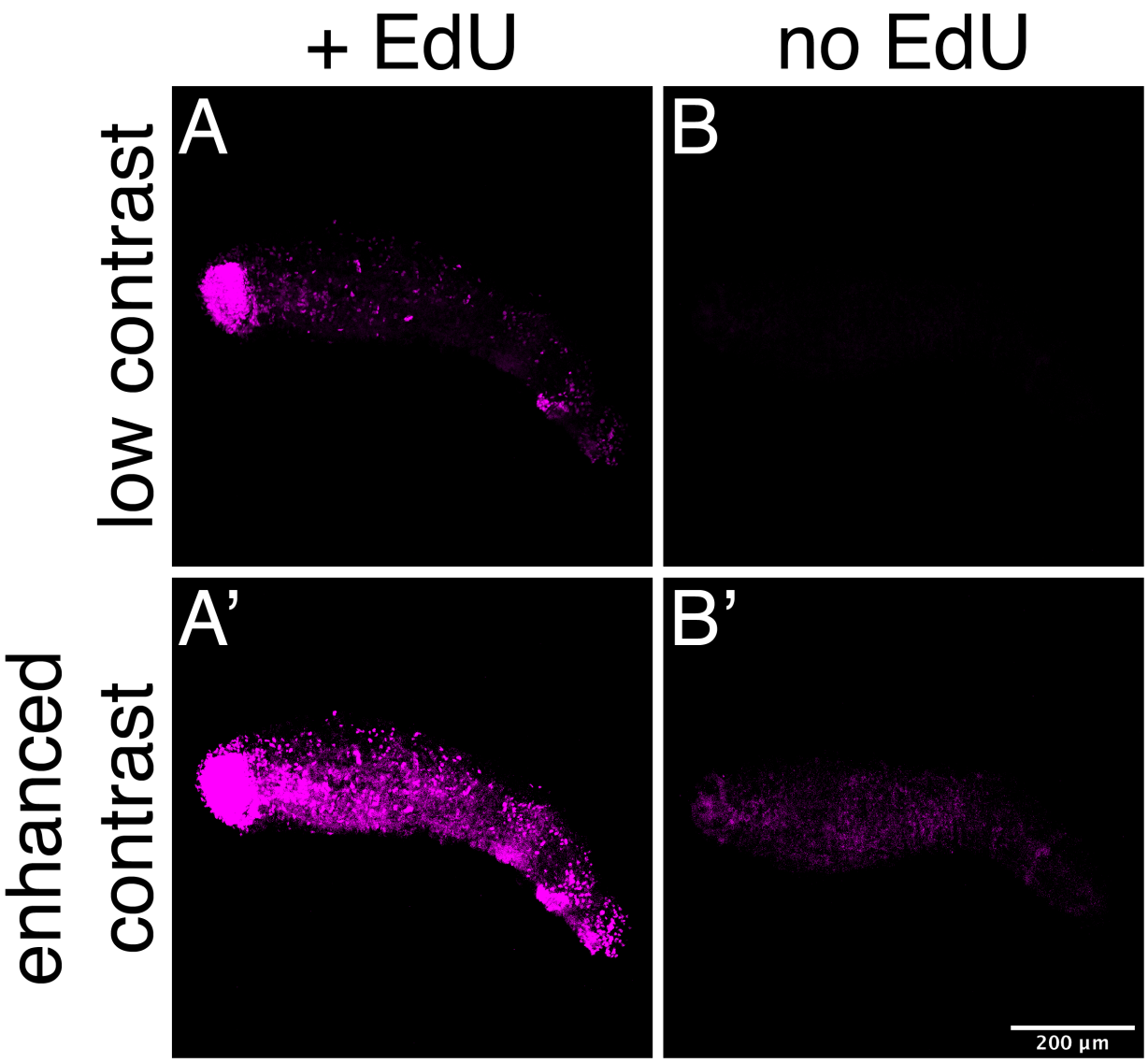

665
666 **Fig. 8. EdU incubation specifically labeled proliferating cells.** The regenerating worms were
667 incubated with or without EdU between 24-48 HPA. Without EdU, background signal appeared
668 only when the contrast of image was highly enhanced (**B'**).
669
670

671 **Table 1.** Degenerate primers initially used to clone Wnt pathway related genes.

Primer name	Sequence
wnt4-F1	CCDCGYGGRCAGCAAAGCA
wnt4-R1	ARTGCAARTGTCATGGHGTG
β-catenin-F1	GTGCGHCTGGCYGGHGGRYTGCA
β-catenin-R1	CRGCYRTVTGTGCTCTTCGTC

672 Code: M = A or C; B = C, G, or T; R = A or G; Y = C or T; V = A, C, or G; H = A, C, or T.

673

674 **Table 2.** Primers for 5' and 3' RACE. Note that *wnt4*-R2 and *β-catenin*-R2 were used as gene
675 specific primers for first strand cDNA synthesis during reverse transcription of 5' RACE.

Primer name	Sequence	Primer partner	Amplification target
3' AP	GGCCACGCGTCGACTAGTACTTTTTT TTTTTTTTTTTT		
3' AP head	GGCCACGCGTCGACTAGTAC		
5' AP	GGCCACGCGTCGACTAGTACGGGG GGGGGGGGGGGG		
5' AP head	GGCCACGCGTCGACTAGTAC		
wnt4-F2	TTCAAAGCGTTGGCACAAGACTGC	3' AP	*wnt4* cDNA and *wnt4* 3' RACE 1st nested PCR
wnt4-F3	TCAAGGCACACGTGACGTTCTACA	3' AP head	*wnt4* 3' RACE 2nd nested PCR
wnt4-R2	GGTGAAGGCACTAGGTACACTAG	5' AP	*wnt4* 5' RACE 1st nested PCR
wnt4-R3	TGTAGAACGTCACGT	5' AP head	*wnt4* 5' RACE 2nd nested PCR
wnt8-F1	GTGGACGAACACTGCGGCTGCA	3' AP	*wnt8* 3' RACE 1st nested PCR
wnt8-F2	GCGTTGCTCTCAGCCAACCGAA	3' AP head	*wnt8* 3' RACE 2nd nested PCR
β-catenin-F2	GATGCTGCTACTAAAGTGGATG	3' AP	*β-catenin* 3' RACE 1st nested PCR
β-catenin-F3	GCAAGAGGGTGCCACAGCTCC	3' AP	*β-catenin* 3' RACE 2nd nested PCR
β-catenin-F4	GACACCGTGGTACGACACGG	3' AP	*β-catenin* 3' RACE 3rd nested PCR
β-catenin-R2	GCCACCAGCTTCAACAACAGCAGG		*β-catenin* cDNA
β-catenin-R3	GTTCACCAGGACCTCCAGAAGCC	5' AP	*β-catenin* 5' RACE 1st nested PCR
β-catenin-R4	TAGCTTGCTTTCTTGGTTACC	5' AP head	*β-catenin* 5' RACE 2nd nested PCR

676

677 **Table 3.** Primers for synthesizing riboprobe templates.

Primer name	Sequence	Target product length (bp)
*wnt4*_ISH-F1	CATGTTGGAGAGCGCTGCC	792
*wnt4*_ISH-R1	CATGTGTATTCGTTGATGTGCAC	
*wnt8*_ISH-F1	CGGAGAGATGGTGAGTCGCCTT	934
*wnt8*_ISH-R1	TGTGCGGGCGTGCTTTGCGTAT	
*β-catenin*_ISH-F1	CGCAATGAAGGAGTTGCCAC	885
*β-catenin*_ISH-R1	TCGTCTACCATGTACACAGG	

678